Biosensors and Bioelectronics: X 13 (2023) 100310

Contents lists available at ScienceDirect

Biosensors and Bioelectronics: X

journal homepage: www.journals.elsevier.com/biosensors-and-bioelectronics-x

Bacterial nanocellulose membrane as novel substrate for biomimetic structural color materials: Application to lysozyme sensing

Akmaral Suleimenova [a,b,d], Manuela F. Frasco [b,*], Francisco A.G. Soares da Silva [c], Miguel Gama [c], Elvira Fortunato [d], M. Goreti F. Sales [a,b,**]

[a] BioMark@ISEP/CEB – LABBELS, School of Engineering, Polytechnic Institute of Porto, Porto, Portugal
[b] BioMark@UC/CEB – LABBELS, Department of Chemical Engineering, Faculty of Sciences and Technology, University of Coimbra, Coimbra, Portugal
[c] CEB – LABBELS, Centre of Biological Engineering, University of Minho, Braga, Portugal
[d] CENIMAT|i3N, Department of Materials Science, School of Science and Technology, NOVA University of Lisbon and CEMOP/UNINOVA, Caparica, Portugal

ARTICLE INFO

Keywords:
Bacterial nanocellulose
Polydopamine
Molecular imprinting technology
Photonic polymers
Lysozyme

ABSTRACT

The development of optical biosensors based on structural colors generated by short-range ordered colloidal particles is attracting growing interest due to their non-iridescent and non-fading features. In this study, a biomimetic approach using biopolymers for the various steps of sensor construction is presented. Bacterial nanocellulose (BNC) has many foreseen applications in biomedical engineering because of its biocompatibility, good mechanical strength, and large modifiable surface area. Herein, a novel approach is taken by using functionalized BNC as a substrate to build a molecularly imprinted photonic sensing layer. BNC was modified with polydopamine (PDA), which improved the adhesion and mechanical properties of the BNC substrate while providing simultaneously a black background for color saturation. A molecularly imprinted polymer (MIP) also made of PDA was used to create the recognition sites for the biomarker lysozyme. A monodisperse colloidal suspension of silica particles was first synthesized and used as core of the MIP shell, and then the photonic structure was assembled on the PDA-BNC membrane. The biosensor showed a detection limit of about 0.8 nmol L^{-1} of lysozyme in spiked human serum and demonstrated to be selective against cystatin C. These properties, combined with biocompatible, eco-friendly, and low-cost materials, offer a sustainable sensing platform with great potential for healthcare applications.

1. Introduction

Label-free optical biosensors are one of the most promising technologies in diagnostics, as they allow rapid and cost-effective detection in small reaction volumes. Within this branch, biosensors based on structural color stand out as they meet all current requirements such as low-cost fabrication, short assay time, and sensitive detection (Inan et al., 2017; Wang et al., 2021). Photonic crystals (PCs) are highly ordered structures with periodic variation in refractive index that modulate the flow of light. PCs occur in biological systems and provide inspiration for the development of synthetic photonic nanocomposite structures (Vukusic and Sambles, 2003). Structural periodicity on the scale of visible light prevents certain wavelengths from propagating through the structure, being reflected and determining the observed color (Inan et al., 2017; Wang et al., 2021). Thus, the ability to precisely control the optical properties, makes PCs very useful for sensing applications. Structural colors resulting from PCs have many unique properties such as iridescence, no photobleaching, and no fading (Dumanli and Savin, 2016; Gur et al., 2015; Zhang et al., 2014).

Although most PC-based biosensors rely on long-range organized crystals, their iridescent or angle dependent colors can be a disadvantage in colorimetric sensors because the color varies depending on the viewing angle, which should not be confused with sensor response (Hu et al., 2021; Y. Zhang et al., 2018a). Thus, short-range coloration arising from amorphous structures is angle-independent and their optical properties are advantageous in this context (Hu et al., 2021). The

* Corresponding author. BioMark@UC/CEB – LABBELS, Department of Chemical Engineering, Faculty of Sciences and Technology, University of Coimbra, Coimbra, Portugal
** Corresponding author. BioMark@UC/CEB – LABBELS, Department of Chemical Engineering, Faculty of Sciences and Technology, University of Coimbra, Coimbra, Portugal
E-mail addresses: mffrasco@gmail.com (M.F. Frasco), goreti.sales@eq.uc.pt, goreti.sales@gmail.com (M.G.F. Sales).

https://doi.org/10.1016/j.biosx.2023.100310
Received 5 December 2022; Received in revised form 16 January 2023; Accepted 29 January 2023
Available online 3 February 2023

coherent scattering in an amorphous structure is easily shielded by random scattering that originates a white appearance. Thus, the underlying structural color is observed by adding materials with light absorbing capacities, which suppresses the random scattering and improves the color saturation (Goerlitzer et al., 2018). The addition of black pigments like carbon black or various polymeric coatings based on polypyrrole and polydopamine (PDA) have been used in the development of materials in seek for structural color saturation (Hu et al., 2021; Hyon et al., 2015; Wei et al., 2010). PDA in small amounts enhances the color gamut and in higher amounts the black color absorbs the scattered light of the photonic structure and improves the color saturation of PCs (Kawamura et al., 2016; Shi et al., 2019; Wei et al., 2010).

Structural coloration can be combined with molecular imprinting technique so that biomimetic biorecognition and signal transduction directly convert the analyte recognition process into a measurable optical label-free signal (Chen et al., 2016). In this approach, the PC structure is usually embedded into a polymerizable mixture of monomers in the presence of the target molecule. After polymerization, the analyte molecules are removed from the polymer matrix leaving behind highly selective recognition nanocavities. Upon rebinding of the analyte, a change in the molecularly imprinted polymer (MIP) resulting from accommodating the target into the cavities induces changes in the reflectance signal of the PC structure (Fenzl et al., 2014). The advantages of PC-MIP sensors are that they are easy to read, cost-effective and relatively simple to construct (Chen et al., 2016). Opal structures derived from self-assembly of colloidal silica particles are a very common starting point to construct PC-MIPs. Such photonic sensors have already been developed for various biomarkers, including proteins like hemoglobin (W. Chen et al., 2015; Zhao et al., 2009), fibrinopeptide (Resende et al., 2020) and bovine serum albumin (Hu et al., 2007).

An important feature in the development of biosensors is sustainability, which creates a need for alternative solutions based on biodegradable materials. In this context, cellulose is one of the most studied biopolymers, which has given rise to numerous paper-based point-of-care devices (Hou et al., 2022; Lee et al., 2021). Another issue is sensor flexibility, as wearable biosensors could be a great solution for real-time health monitoring. Substrates based on cellulose and its derivatives can meet all these requirements for sensor development because these materials are simple, abundant, inexpensive, biodegradable, and flexible. Biosensors on cellulose paper offer additional advantages such as ease of use, accuracy, and rapid response (Kamel and Khattab, 2020).

Bacterial nanocellulose (BNC) is a sustainable alternative (Forte et al., 2021) to its plant derived counterpart, since it can be obtained by fermentation from byproducts of the food industry using *e.g. Komagataeibacter sucrofermentans* (Cielecka et al., 2019). When produced by static culture, it presents a unique three-dimensional nanofiber network, which cannot be obtained from other sources of cellulose. This material features a large surface area associated to a highly porous structure, which makes possible a rapid diffusion of molecules through the mesh and a good dispersion of chemicals, with high absorption capacity (Iguchi et al., 1991). These properties provide a higher sensitivity and accuracy when BNC is used as a matrix for analytical applications (Andrade et al., 2010). In addition, there are a large number of reactive hydroxyl groups on the surface that are suitable for chemical modification and better attachment of sensing material (Gu and Dichiara, 2020).

In this work, BNC was used for the first time as a substrate for the construction of an optical biosensor based on structural color. The surface-adhesion and color enhancing properties of PDA were used both as a coating of BNC and as a core-shell MIP. Colloidal silica particles were used to fabricate the PDA shell with the imprinted recognition sites for the protein target, followed by self-assembly of the MIP spheres on PDA-BNC membrane (Fig. 1). Thus, the combination of eco-friendly materials and biopolymers used to fabricate the current sensor meet the desired criteria of biodegradability and biocompatibility, which are of interest for the development of future flexible optical devices. Lysozyme was selected as the protein biomarker for proof-of-concept. Lysozyme is a ubiquitous enzyme present in human fluids (e.g., serum, urine, tears) and is therefore a well-studied biomarker known to be "body's own antibiotic" because of its antimicrobial activities (Hanstock et al., 2019; Zhang et al., 2020). Due to the immunomodulatory ability of lysozyme, its altered levels have been reported as a useful biomarker for cancer, kidney disfunction, sarcoidosis, and cardiovascular diseases (Abdul-Salam et al., 2010; Jiang et al., 2021; Sahin et al., 2016). The presence of lysozyme on the surface of human plasma extracellular vesicles has been also reported, suggesting that it is involved in intercellular communication in stress-induced intestinal damage, related to cell repair and inflammatory responses (Abey et al., 2017).

2. Material and methods

2.1. Reagents

All chemicals were of analytical grade and used without further

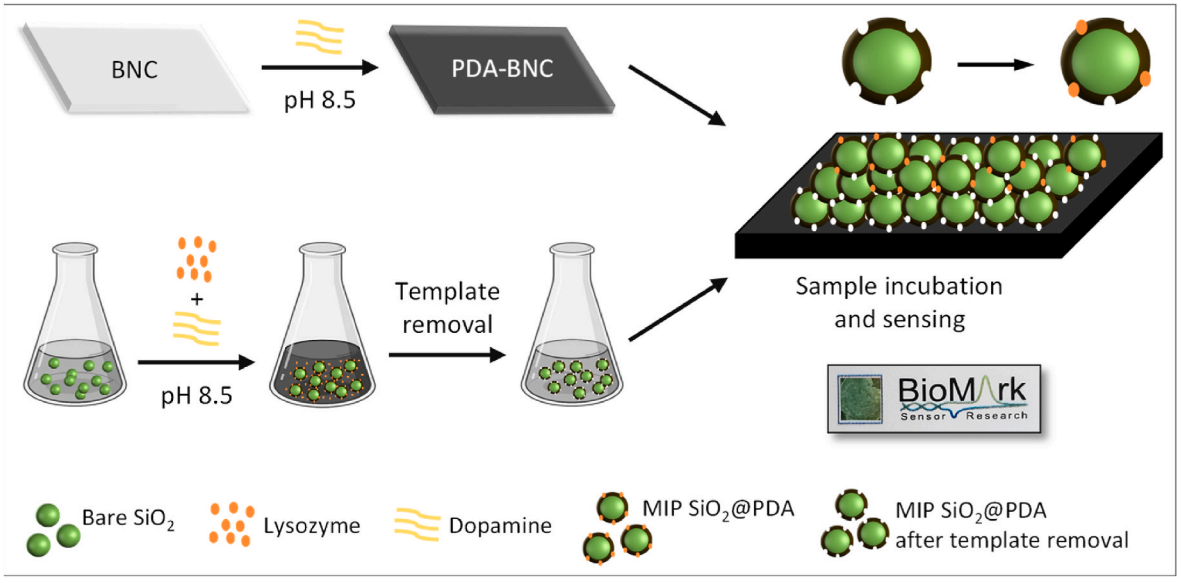

Fig. 1. Schematic representation of the sensor design and assembly.

purification. Tetraethoxysilane (TEOS) 99% and 3-Hydroxytyramine chloride for synthesis were purchased from Merck. Ammonium hydroxide 25%, was obtained from Fluka. Ethanol absolute ≥99.9%, lysozyme and cystatin C were purchased from Sigma-Aldrich. Cormay Serum HN was bought from PZ Cormay S.A. Phosphate Buffered Saline (PBS) tablets were acquired from VWR and Tris (hydroxymethyl)aminomethane was obtained from Fisher BioReagents. Ultrapure laboratory grade water was used (conductivity ≤0.06 μS cm^{-1}).

2.2. Preparation of polydopamine (PDA) functionalized bacterial nanocellulose (BNC)

BNC was obtained through synthesis from bacteria *Komagataeibacter sucrofermentans* as previously described (Soares da Silva et al., 2022). The sponge-like BNC matrix (2 cm × 2 cm) was immersed at 10 mmol L^{-1} of dopamine in Tris buffer 10 mmol L^{-1} pH 8.5 for 48 h under agitation (100 rpm), at room temperature. Then, the functionalized PDA-BNC matrix was placed under a press and totally dried at 30 °C.

2.3. Preparation of sensing molecularly imprinted polymer (MIP)

First, highly monodisperse silica particles were synthesized using the modified Stöber method (Stöber et al., 1968). Solution A was obtained by mixing 8 mL of ammonia, 62 mL of ethanol absolute, and 3 mL of ultrapure water. Solution B was obtained by mixing 6 mL of TEOS and 21 mL of ethanol absolute. Solution B was quickly added to solution A under 900 rpm stirring and slowed down after 5 min to 600 rpm for 2 h at 60 °C. The obtained colloidal dispersion was centrifuged (7000 rpm, 10 min) and washed with ethanol several times. The obtained silica spheres were dispersed in ultrapure water and stored for further usage and characterization.

The formation of the MIP shell around silica particles was made via *in situ* polymerization technique. Thus, a dispersion of silica particles (~0.9 mg mL^{-1}) was mixed with dopamine (10 mmol L^{-1}) and with lysozyme (1000 nmol L^{-1}) in Tris buffer (10 mmol L^{-1}, pH 8.5). The mixture was left to react for 30 min under stirring (1000 rpm), followed by several rounds of centrifugation (7000 rpm, 10 min) and resuspension in ultrapure water to remove non-polymerized dopamine and free PDA. The washing process was monitored by UV–Vis spectroscopy until no PDA was detected in the supernatant. The MIP particles were then incubated 2 h in ethanol to remove the template lysozyme from the imprinted matrix.

2.4. Sensor assembly and analytical performance

The sensors were assembled via drop-casting of a mixture of bare silica particles in ethanol and the core-shell MIP SiO_2@PDA in water on the surface of PDA-BNC (5 mm × 5 mm) in 1:2 proportion, and subsequently dried at room temperature. To obtain the analytical data, at least three independent replicates using independent sensors were performed, and results are presented as average with standard error. The response of the sensors was first evaluated in PBS buffer (10 mmol L^{-1}, pH 7.4). To assess if the sensors maintained a relatively stable and repeatable signal under multiple measurements, they were assayed after successive 30 min incubations with PBS buffer for 180 min. The signal fluctuations were below 5% (n = 5) for any tested time regarding the initial levels. Thus, the sensors were considered stable, and the calibration studies proceeded. For each calibration, the sensor was first equilibrated with PBS buffer for 30 min, and then lysozyme (1 nmol L^{-1} to 100 nmol L^{-1}) was successively incubated by drop casting on the sensor for 30 min in a wet chamber. After washing and drying, reflectance spectra were obtained. Then, a similar procedure was performed in serum diluted 1000-fold in PBS buffer, by testing the same lysozyme concentrations (1 nmol L^{-1} to 100 nmol L^{-1}) prepared in diluted serum. Sensor responses were analyzed by the relative area under the curve (AUC), i.e. AUC/AUC_0, where AUC_0 is the blank and AUC corresponds to each protein standard. Calibration plots of the optical signal against the logarithm concentration of lysozyme were evaluated regarding the linear regression obtained. The limit of detection (LOD) was calculated following IUPAC procedure for logarithm dependent calibrations (Buck and Lindner, 1994).

For the selectivity tests, the recognition of lysozyme was measured against cystatin C in spiked serum (1000-fold diluted in PBS buffer). The sensor response to cystatin C in low (0.1 nmol L^{-1}) and high (10 nmol L^{-1}) levels was evaluated separately or in combination with lysozyme, also for both low (2.1 nmol L^{-1}) and high (55 nmol L^{-1}) concentrations. The accuracy of the sensor was evaluated in 1000-fold diluted serum spiked with the two concentrations (2.1 and 55 nmol L^{-1}) of lysozyme.

2.5. Characterization

Scanning electron microscope (SEM) images were taken on FEI Quanta 400 FEG ESEM equipment. The hydrodynamic diameter, polydispersity index, and zeta potential of silica spheres and sensing materials were analyzed by dynamic light scattering (DLS) using a Malvern Zetasizer Nano ZS (Malvern Instruments Ltd., UK). Reflectance spectra were taken on Ocean Optics DH2000 spectrometer in reflection mode. The optical set up comprised a reflection fiber probe (fiber diameter of 200 μm, Ocean Optics), and halogen light source along with Ocean optic Flame miniature spectrometer. A diffuse reflectance standard was used for white background with halogen light source on and off for black background.

3. Results and discussion

3.1. Preparation of PDA-BNC

The isolated BNC is a soft membrane with high water holding capacity (Fig. 2A) and shows characteristic native 3D nanofibrillar structures when observed by SEM (Fig. 2B) (Fernandes et al., 2019). BNC applications are vast (Lokhande et al., 2022; Rai and Dhar, 2022), but the combination of BNC with PDA has been less studied. The highly attractive properties of PDA considering its biocompatibility, biodegradability, and high photothermal conversion efficiency makes PDA-BNC membranes very useful to develop photothermal materials, for water treatment, and for wound healing by having anti-bacterial properties (Jiang et al., 2017; Jun et al., 2019; Li et al., 2022; Wahid et al., 2021). In the present work, BNC was immersed in dopamine solution while polymerization occurred. The oxidative self-polymerization of dopamine is a well-known process to obtain PDA (Postma et al., 2009), and this process was optimized in the current work to efficiently trap PDA particles in BNC matrix. Representative photos of PDA-BNC membranes in wet (Fig. 2C) and press-dried (Fig. 2D) states show that flexible black membranes were obtained. Thus, the PDA particles were efficiently incorporated in the BNC fiber network (Fig. 2E and F). As observed in the SEM images, the size of PDA particles was not uniform, but that did not compromise the desired properties of the membrane since the particles did not leach out of the BNC fibers. BNC polysaccharide contains free hydroxyl groups that may establish numerous hydrogen bonds with PDA to generate the coating (Wahid et al., 2021).

Using this approach, the native high tensile strength properties of BNC were combined with biomimetic mussel-like surface-adhesion features of PDA, resulting in biodegradable with slight stretching capacity membranes. Moreover, the black color of PDA-BNC membranes makes them ideal substrates to integrate structural color-based reflectance sensing materials.

3.2. Preparation of sensing MIP on silica particles

The sensing MIP was designed based on a core-shell strategy having silica particles as a starting material. The synthesized silica particles had around 240 nm in size, as observed in SEM (Fig. 3A). The size and

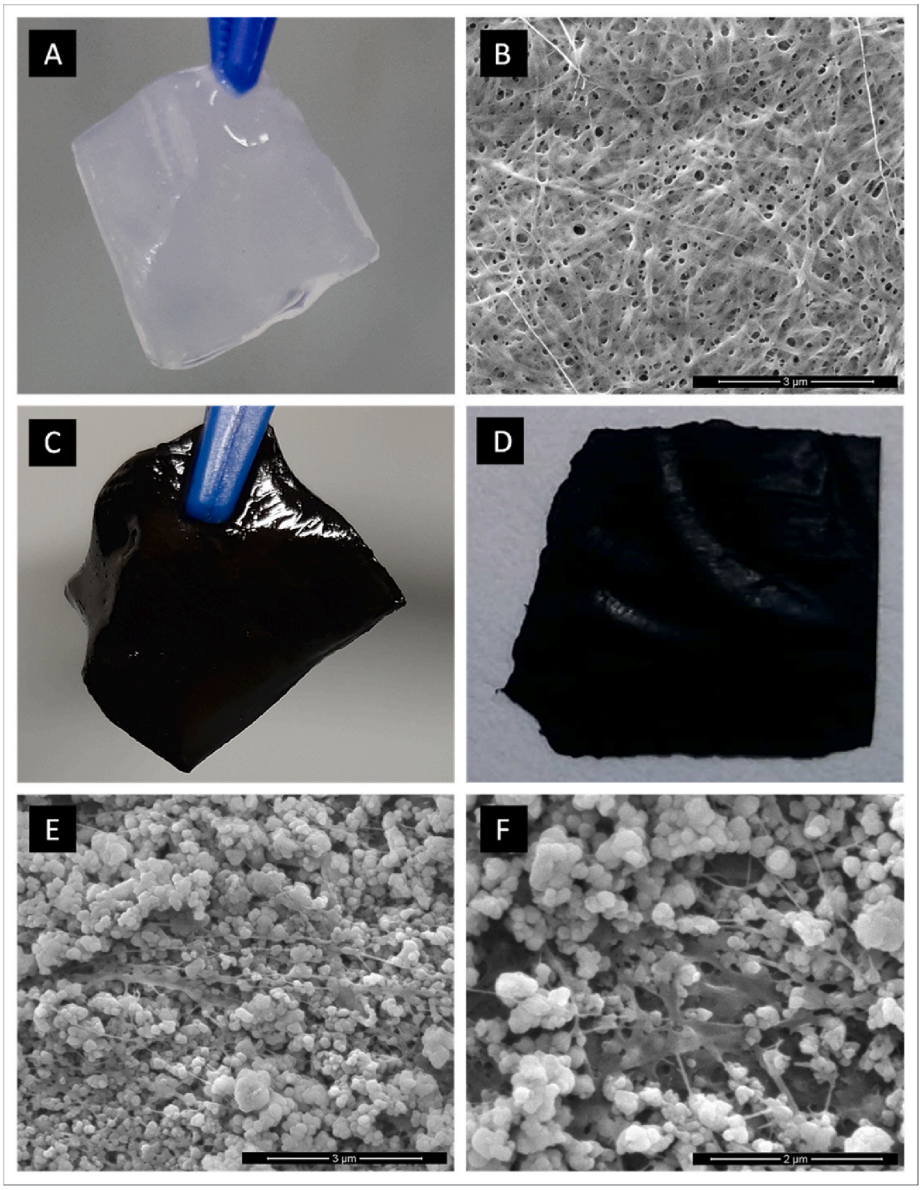

Fig. 2. Photograph of pristine BNC (A) and its fiber network as observed by SEM (B), and subsequent modification with PDA, resulting in black membranes in wet (C) and dried (D) states, with SEM characterization showing PDA particles within BNC fibers (E, F).

monodispersity were confirmed by DLS (Fig. 3D). The DLS measurements suggest that a narrow particle size distribution (PDI of 0.02 ± 0.01) (Danaei et al., 2018) of 264.4 ± 1.4 nm diameter was obtained. The difference in size in comparison to SEM was expected because the hydrodynamic size includes the solvation shell (He et al., 2012). The particles had a negative surface charge of −46.2 ± 0.4 mV, as showed by zeta potential measurements (Fig. 3D), indicating that the dispersion is stable due to electrostatic repulsion between the particles due to surface hydrophilic silanol groups.

Among the many configurations used for MIP preparation, core-shell MIP particles have been greatly studied particularly due to the possibility of integrating MIPs with other functional components and for improving MIP performance (e.g., better recognition by reduced mass transfer resistance) (Wan et al., 2017). Interestingly, PDA has been described as good polymer matrix for molecular imprinting of proteins (J. Chen et al., 2015; Xia et al., 2013; Yang et al., 2016)). In the current study, the shell of PDA is aimed for improved interaction with PDA-BNC substrate and for optical tuning of the structural color, besides providing recognition sites for lysozyme detection. After extensively washing the MIP particles, including for template removal, the visual observation that the initial milky-white solution of silica particles turned brown was the first indication that a successful core-shell structure was formed. Upon SEM analysis, the images show an effective formation of PDA shell because the spherical shape is more irregular (Fig. 3B) in comparison to bare silica particles (Fig. 3A). Both MIP and NIP control (Fig. 3C) presented the same morphology. In terms of size, SEM and DLS analyses did not show a significant difference in comparison to bare silica particles Nevertheless, DLS results indicated that the imprinted layers would have around 5 nm, which is in accordance with the literature (Kawamura et al., 2016; Xia et al., 2013). In addition, MIP (and NIP) maintained a relatively low polydispersity index (PDI). The presence and stability of the imprinted PDA layer was further confirmed by the zeta potential value since the surface charge became less negative after the PDA shell (Fig. 3D).

3.3. Sensor assembly on PDA-BNC

PDA films have been used to create surface-adherent mussel-inspired

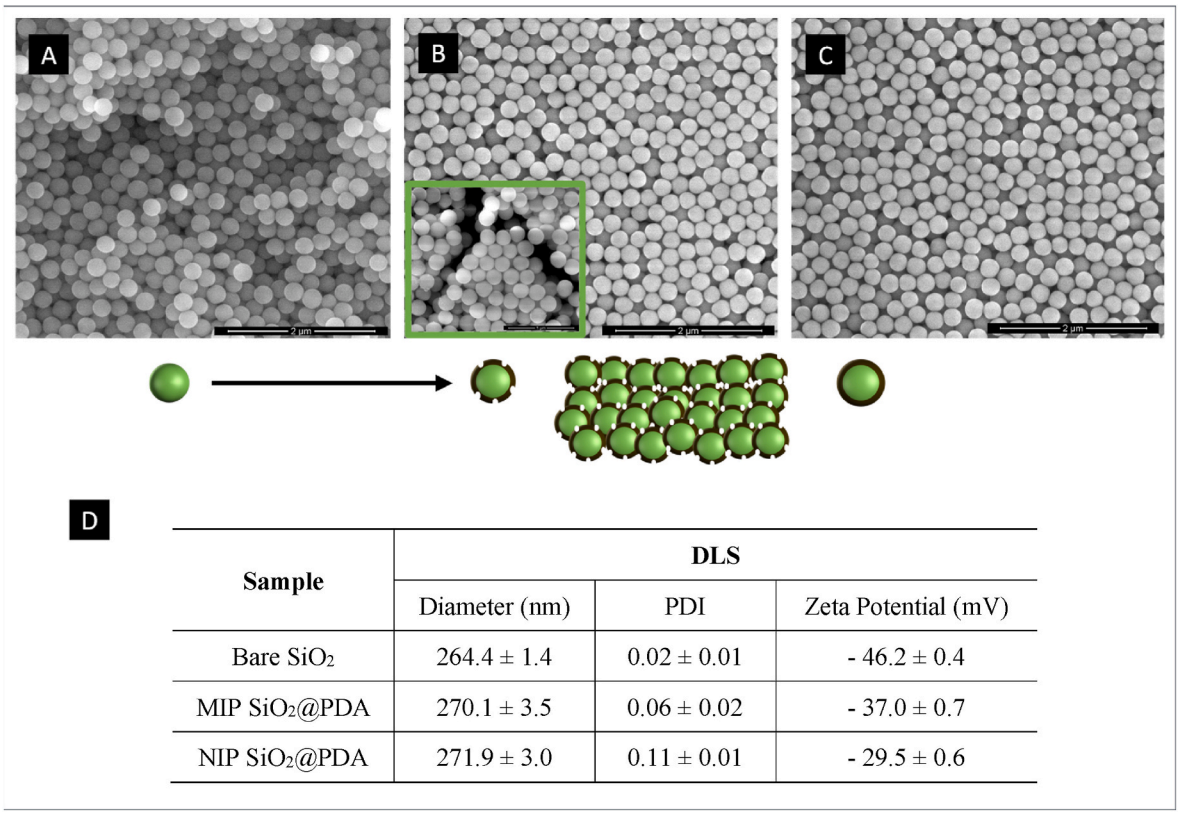

D

Sample	DLS		
	Diameter (nm)	PDI	Zeta Potential (mV)
Bare SiO_2	264.4 ± 1.4	0.02 ± 0.01	- 46.2 ± 0.4
MIP SiO_2@PDA	270.1 ± 3.5	0.06 ± 0.02	- 37.0 ± 0.7
NIP SiO_2@PDA	271.9 ± 3.0	0.11 ± 0.01	- 29.5 ± 0.6

Fig. 3. Characterization by SEM (A–C) and by DLS (D). Bare silica particles after synthesis (A), MIP (B) and NIP (C) after self-assembly on PDA-BNC. The SEM image of MIP shows an inset representing the quasi-amorphous structure of the obtained structure (B).

coatings (Lee et al., 2007; Loget et al., 2015). The unique adhesive properties of PDA helped improving the assembly of the sensor on the PDA-BNC substrate since both surfaces were coated with PDA. In addition, it allowed to modulate the fabrication of a colorimetric sensor by non-iridescent structural color. The addition of absorbing materials like PDA, carbon black or black polypyrrole to modify PC structures and make them non-iridescent, i.e., the observed colors become angle-independent, has been explored for some applications (Xiao et al., 2017). Moreover, color saturation due to absorbing incoherent scattering can be modulated. For example, by creating different thicknesses of PDA on polystyrene spheres, the blackness and refractive index of the colloidal particles could be successfully controlled (Kawamura et al., 2016) In the current strategy, the assembly of the MIP (and respective NIP control) originated a short-range order photonic quasi-amorphous structure (Fig. 3B and C). The colloidal MIPs were deposited on the PDA-BNC followed by solvent evaporation. Usually, there is a strong colloidal crystallization tendency during the assembly process (Hu et al., 2019). Thus, several methods have been proposed to overcome the challenge of creating such amorphous photonic structures (Hu et al., 2021; Liu et al., 2019). Herein, the rough surface of the PDA shell composing the MIP and the PDA-BNC substrate favors the amorphous structure. Nevertheless, for sensing purposes it was convenient to avoid color dependence on the view angle, to have PDA adherence properties, but also to maintain some degree of crystallinity to improve the reflectance signal. This was achieved by assembling the sensing MIP in a mixture with bare silica particles, and the ratio 1:2 of silica particles to MIP was the one that provided the best sensitivity in terms of optical response of the sensor.

3.4. Optical response of MIP

Consecutive additions of lysozyme prepared in PBS buffer resulted in significant decrease of the optical intensity of MIP reflectance proportional to the increase in lysozyme concentration (Fig. 4A). The reflectance of the NIP control showed a slight decrease that was constant with increasing concentrations of lysozyme, suggesting that a non-specific adsorption occurred (Fig. 4B). On the other hand, the MIP had a linear response ($R^2 = 0.991$) between 1 and 100 nmol L^{-1} (slope = −0.206, abscissa = 0.892) (Fig. 4C). The standard error of the slope was 1.15%, confirming the repeatability of the sensors in the linear range. In addition, the obtained LOD in buffer was 0.81 nmol L^{-1}. These results suggest that the response obtained in the imprinted matrix was due to specific recognition cavities tailored for lysozyme on the shell surface of the particles. Empty imprinted sites in the polymer were increasingly occupied by the target protein lowering the refractive index contrast, together with a positive change in the average refractive index and thus leading to reduction in peak intensity (Phillips et al., 2016; Wang et al., 2021). This behavior is consistent with previous works using PCs for detection of other target analytes (Endo et al., 2010; Liu et al., 2012; Zhou et al., 2012).

The behavior of the sensing material was then assayed in the more complex serum matrix. The MIP was tested in the same range of lysozyme concentrations as in PBS buffer and showed a linear decrease in reflectance intensity with increasing protein levels (Fig. 4D). The NIP control also showed an initial decrease in reflectance intensity that was kept almost constant when incubating with increasing concentrations of lysozyme (Fig. 4E). This result suggests the occurrence of non-specific adsorption in NIP material, but the MIP kept its recognition ability (Fig. 4F) achieving a LOD of 0.77 nmol L^{-1}, with good linearity ($R^2 = 0.985$) between 1 and 100 nmol L^{-1}. The LOD obtained in serum was approximately the same as in PBS buffer, but the slope of the curve was slightly lower (slope = −0.174, abscissa = 0.804), suggesting that the presence of other biological components in human serum may impact upon the background signal. Nevertheless, the standard error of the slope was 1.24% in serum, similar to the result obtained in buffer, demonstrating excellent repeatability of the sensors. Thus, in the tested

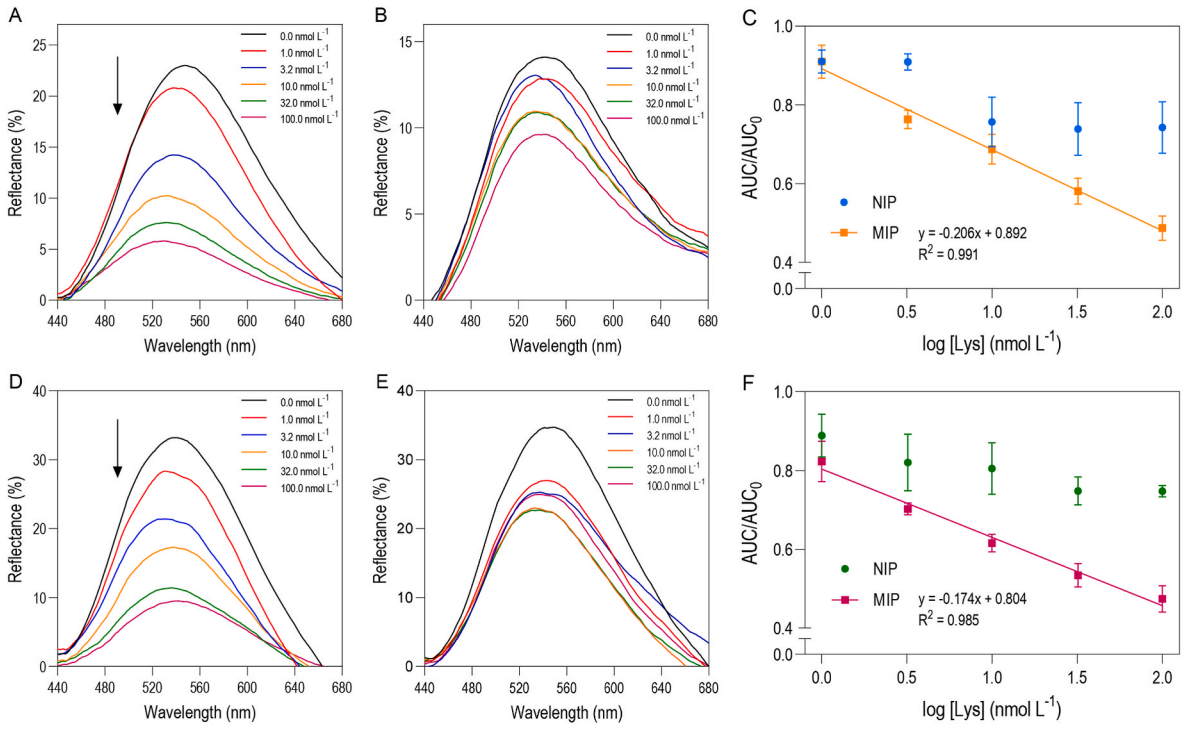

Fig. 4. Analytical performance of MIP@PDA@BNC in 10 mmol L^{-1} PBS buffer pH 7.4 (A–C) and in serum (1000-fold diluted in PBS buffer) (D–F); A, D – representative reflectance spectra of MIP@PDA@BNC; B, E – representative reflectance spectra of NIP@PDA@BNC; C, F – calibration curves with increasing concentrations of lysozyme (Lys), 1 nmol L^{-1} to 100 nmol L^{-1} (n = 3).

conditions, the complexity of the serum did not significantly impair the sensor response.

According to previous studies, the levels of lysozyme in serum of healthy individuals, considering 1000-fold diluted serum, would be around 0.67–1.2 nmol L^{-1}, and increased levels have been reported in a number of diseases including cancer (Johansson and Malmquist, 1971; Luger et al., 1979; Sahin et al., 2016). Thus, the developed photonic MIP sensor could be applied to distinguish healthy from diseased conditions.

Other optical sensors have been previously designed to detect lysozyme, as summarized in Table 1. The sensor described in the current study enabled to achieve a lower LOD of ~0.8 nmol L^{-1} (~11 ng mL^{-1}), in comparison to alternative MIP particles and photonic based optical biosensors in the literature. These good results are in the range of the LOD (5 ng mL^{-1}) obtained when a core-shell MIP was combined with surface-enhanced Raman scattering, known to be an ultrasensitive method (Ren et al., 2020).

In addition, the use of lysozyme imprinted particles has been explored as probes for in vitro sensing of live cells and in controlled release studies (J. Chen et al., 2015; Fang et al., 2019). Particularly, a PDA-MIP for lysozyme was combined with a magnetic core on silica particles to obtain a NIR-light responsive MIP for extraction and controlled release of the biomacromolecule owing to the photothermal effect of the PDA layer (J. Chen et al., 2015). These studies reveal the broaden potential and applications of the materials like those developed in the current sensor.

3.5. Selectivity and accuracy

The selectivity of the developed MIP sensor for lysozyme detection in human serum was evaluated against cystatin C. The protein cystatin C was chosen as potential interferent because its level in serum has been considered a suitable biomarker for cancer diseases (Guo et al., 2017; Leto and Sepporta, 2020). Moreover, both lysozyme and cystatin C share properties in terms of size (cystatin C is 13.3 kDa while lysozyme is 14.3 kDa) and isoelectric point (cystatin C is 9.3 and lysozyme is 11.1) (Okada, 2017; Wu et al., 2015). Thus, it is interesting to understand if the detection of lysozyme in serum can be affected by the presence of cystatin C. Thus, the response of the sensor was evaluated using low and high concentrations of both proteins. Human serum 1000-fold diluted was spiked with lysozyme and cystatin C separately or mixed (Fig. 5). In

Table 1
Comparison of the proposed method with previously reported optical sensors for detection of lysozyme.

Nanostructured materials	Detection	LOD	Ref.
MIP particles based on poly (ethylene-*co*-vinyl alcohol)/ quantum dot composites	Fluorescence quenching	(1) 210 ng mL^{-1} (2) 13 ng mL^{-1}	(1) Lin et al. (2009) (2) Lee et al. (2010)
Silica cross-linked MIP particles containing quantum dots	Fluorescence intensity	3200 ng mL^{-1}	Wang et al. (2022)
Hydrogel imprinted membrane containing quantum dots	Fluorescence quenching	10.2 nmol L^{-1}	X. Zhang et al. (2018b)
Magnetic nanoparticles - quantum dot nanocomposites with MIP shell	Fluorescence quenching	4.53 nmol L^{-1}	Zhang et al. (2021)
MIP-coated carbon dots - silica composite particles	Fluorescence quenching	550 ng mL^{-1}	Fang et al. (2019)
3D opal structure by assembly of polymer brush-grafted silica particles	Shift in the reflection peak	5000 ng mL^{-1}	Chen et al. (2017)
2D photonic crystal hydrogel	Debye diffraction ring	1380 ng mL^{-1}	Wang et al. (2020)
2D photonic hydrogel modified with an aptamer	Debye diffraction ring	1.8 nmol L^{-1}	Shen et al. (2022)
Silver microspheres with MIP shell	Surface-enhanced Raman scattering	5 ng mL^{-1}	Ren et al. (2020)
Polydopamine based MIP on silica particles as a short-range photonic structure	Reflectance decrease	0.8 nmol L^{-1}	This work

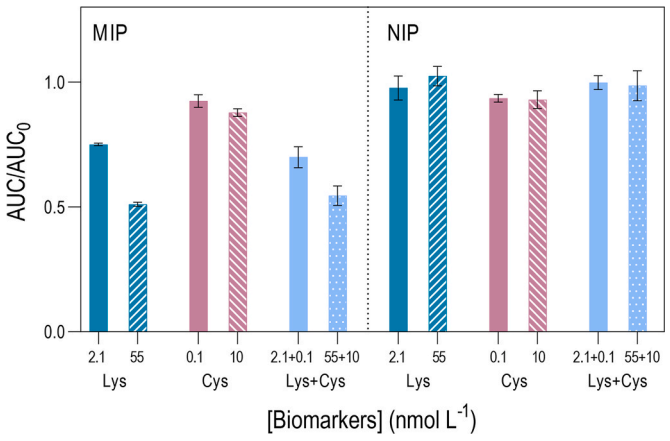

Fig. 5. Selectivity of the MIP sensing layer, and respective NIP control, to single solutions of lysozyme (Lys) and cystatin C (Cys) and to mixed solutions of both proteins at two different concentrations (proteins were prepared in 1000-fold diluted serum) (n = 3).

comparison to the expected decrease in reflectance intensity observed for lysozyme (2.1 and 55 nmol L^{-1}), the optical signal of the MIP sensor did not present a significant change for both tested concentrations of cystatin C (0.1 and 10 nmol L^{-1}) (Fig. 5). The optical signal of the NIP in the presence of cystatin C was similar to MIP, thus suggesting that negligible signal change could result from non-specific adsorption. Moreover, when MIP sensor was incubated with mixed proteins, the presence of cystatin C did not seem to hamper the detection of lysozyme (Fig. 5). The selectivity studies suggest that the imprinted sites play a key role in the recognition process of lysozyme, i.e., the PDA matrix provided the required complementary sites in terms of size, shape and chemical bonds that enabled the sensor to selectivity recognize lysozyme. In addition, the recovery assays were performed after spiking 1000-fold diluted serum with 2.1 and 55 nmol L^{-1} of lysozyme. Regarding the lowest concentration of 2.1 nmol L^{-1}, the measured value shifted −3.5% of the theoretical concentration with a relative standard deviation (RSD) of 10.6% (n = 3), while for the highest value of 55 nmol L^{-1}, the shift was −10.3% with RSD of 19.0% (n = 3). Thus, the measured values were consistent with the spiked levels suggesting an accurate determination of lysozyme within the concentration range under analysis.

4. Conclusions

In this work, environmentally friendly materials such as BNC and PDA were used to construct a lysozyme biosensor based on MIP recognition and short-range photonic structure as transducer element. To the best of our knowledge, this is the first work using a short-range photonic structure assembled on BNC for sensing applications in a biological matrix at clinically relevant levels. The straightforward approach of biosensor design, label-free detection and flexible substrate can open new perspectives for future implementation at the point-of-care. The photonic MIP sensor showed low LOD, and selective detection of lysozyme compared to cystatin C, another cancer biomarker. The low detection limit and linear response, which included healthy and diseased ranges of lysozyme in serum, enable the use of this sensor in various stages of disease and treatment monitoring. Moreover, BNC is a flexible biodegradable substrate that can be easily functionalized and manipulated. Therefore, combining it with other biopolymers, imprinting technology and structural coloration is suitable for the development of low-cost and disposable biosensors without losing the requirements of sensitive detection and sustainability.

Credit author statement

Akmaral Suleimenova. Investigation. Methodology. Validation. Formal analysis. Data curation. Visualization. Writing – original draft. Manuela F. Frasco. Conceptualization. Methodology. Visualization. Supervision. Project administration. Writing – review & editing. Francisco A. G. Soares da Silva. Investigation. Writing – review & editing. Miguel Gama. Resources. Supervision. Writing – review & editing. Elvira Fortunato. Supervision. Writing – review & editing. M. Goreti F. Sales. Methodology. Supervision. Funding acquisition. Project administration. Writing – review & editing.

Declaration of competing interest

The authors declare that they have no known competing financial interests or personal relationships that could have appeared to influence the work reported in this paper.

Data availability

Data will be made available on request.

Acknowledgements

The authors gratefully acknowledge funding from the European Commission through the project MindGAP (FET-Open/H2020/GA829040). The author Akmaral Suleimenova acknowledges the MIT Portugal PhD grant (PD/BD/142776/2018) funded by Fundação para a Ciência e a Tecnologia (FCT).

References

Abdul-Salam, V.B., Ramrakha, P., Krishnan, U., Owen, D.R., Shalhoub, J., Davies, A.H., Tang, T.Y., Gillard, J.H., Boyle, J.J., Wilkins, M.R., Edwards, R.J., 2010. Identification and assessment of plasma lysozyme as a putative biomarker of atherosclerosis. Arterioscler. Thromb. Vasc. Biol. 30, 1027–1033. https://doi.org/10.1161/ATVBAHA.109.199810.

Abey, S.K., Yuana, Y., Joseph, P.V., Kenea, N.D., Fourie, N.H., Sherwin, L.B., Gonye, G.E., Smyser, P.A., Stempinski, E.S., Boulineaux, C.M., Weaver, K.R., Bleck, C.K.E., Henderson, W.A., 2017. Lysozyme association with circulating RNA, extracellular vesicles, and chronic stress. BBA Clin 7, 23–35. https://doi.org/10.1016/j.bbacli.2016.12.003.

Andrade, F.K., Pertile, R., Dourado, F., Gama, F.M., 2010. Bacterial Cellulose: Properties, Production and Applications. In: Lejeune, A., Deprez, T. (Eds.), Cellulose: Structure and Properties, Derivatives and Industrial Uses. Nova Science Publishers Inc, ISBN 978-1-60876-388-7, pp. 427–458.

Buck, R.P., Lindner, E., 1994. Recommendations for nomenclature of ionselective electrodes (IUPAC Recommendations 1994). Pure Appl. Chem. 66, 2527–2536. https://doi.org/10.1351/pac199466122527.

Chen, J., Lei, S., Xie, Y., Wang, M., Yang, J., Ge, X., 2015. Fabrication of high-performance magnetic lysozyme-imprinted microsphere and its NIR-responsive controlled release property. ACS Appl. Mater. Interfaces 7, 28606–28615. https://doi.org/10.1021/acsami.5b10126.

Chen, W., Meng, Z., Xue, M., Shea, K.J., 2016. Molecular imprinted photonic crystal for sensing of biomolecules. Mol. Imprinting 1–12. https://doi.org/10.1515/molim-2016-0001.

Chen, W., Shea, K.J., Xue, M., Qiu, L., Lan, Y., Meng, Z., 2017. Self-assembly of the polymer brush-grafted silica colloidal array for recognition of proteins. Anal. Bioanal. Chem. 409, 5319–5326. https://doi.org/10.1007/s00216-017-0477-5.

Chen, W., Xue, M., Shea, K.J., Meng, Z., Yan, Z., Wang, Z., Xue, F., Qu, F., 2015. Molecularly imprinted hollow sphere array for the sensing of proteins. J. Biophot. 8, 838–845. https://doi.org/10.1002/jbio.201400100.

Cielecka, I., Szustak, M., Kalinowska, H., Gendaszewska-Darmach, E., Ryngajłło, M., Maniukiewicz, W., Bielecki, S., 2019. Glycerol-plasticized bacterial nanocellulose-based composites with enhanced flexibility and liquid sorption capacity. Cellulose 26, 5409–5426. https://doi.org/10.1007/s10570-019-02501-1.

Danaei, M., Dehghankhold, M., Ataei, S., Hasanzadeh Davarani, F., Javanmard, R., Dokhani, A., Khorasani, S., Mozafari, M.R., 2018. Impact of particle size and polydispersity index on the clinical applications of lipidic nanocarrier systems. Pharmaceutics 10, 57. https://doi.org/10.3390/pharmaceutics10020057.

Dumanli, A.G., Savin, T., 2016. Recent advances in the biomimicry of structural colours. Chem. Soc. Rev. 45, 6698–6724. https://doi.org/10.1039/C6CS00129G.

Endo, T., Ozawa, S., Okuda, N., Yanagida, Y., Tanaka, S., Hatsuzawa, T., 2010. Reflectometric detection of influenza virus in human saliva using nanoimprint lithography-based flexible two-dimensional photonic crystal biosensor. Sensor. Actuator. B Chem. 1, 269–276. https://doi.org/10.1016/j.snb.2010.05.036.

Fang, M., Zhuo, K., Chen, Y., Zhao, Y., Bai, G., Wang, J., 2019. Fluorescent probe based on carbon dots/silica/molecularly imprinted polymer for lysozyme detection and cell imaging. Anal. Bioanal. Chem. 411, 5799–5807. https://doi.org/10.1007/s00216-019-01960-6.

Fenzl, C., Hirsch, T., Wolfbeis, O.S., 2014. Photonic crystals for chemical sensing and biosensing. Angew. Chem., Int. Ed. Engl. 53, 3318–3335. https://doi.org/10.1002/anie.201307828.

Fernandes, M., Gama, M., Dourado, F., Souto, A.P., 2019. Development of novel bacterial cellulose composites for the textile and shoe industry. Microb. Biotechnol. 12, 650–661. https://doi.org/10.1111/1751-7915.13387.

Forte, A., Dourado, F., Mota, A., Neto, B., Gama, M., Ferreira, E.C., 2021. Life cycle assessment of bacterial cellulose production. Int. J. Life Cycle Assess. 26, 864–878. https://doi.org/10.1007/s11367-021-01904-2.

Goerlitzer, E.S.A., Klupp Taylor, R.N., Vogel, N., 2018. Bioinspired photonic pigments from colloidal self-assembly. Adv. Mater. 30, 1706654 https://doi.org/10.1002/adma.201706654.

Gu, J., Dichiara, A., 2020. Hybridization between cellulose nanofibrils and faceted silver nanoparticles used with surface enhanced Raman scattering for trace dye detection. Int. J. Biol. Macromol. 143, 85–92. https://doi.org/10.1016/j.ijbiomac.2019.12.018.

Guo, S., Xue, Y., He, Q., He, X., Guo, K., Dong, P., Yao, K., Yang, G., Chen, D., Li, Z., Li, X., Qin, Z., Liu, Z., Cheng, W., Guo, C., Zhang, M., Han, H., Zhou, F., 2017. Preoperative serum cystatin-C as a potential biomarker for prognosis of renal cell carcinoma. PLoS One 12, e0178823. https://doi.org/10.1371/journal.pone.0178823.

Gur, D., Leshem, B., Pierantoni, M., Farstey, V., Oron, D., Weiner, S., Addadi, L., 2015. Structural basis for the brilliant colors of the sapphirinid copepods. J. Am. Chem. Soc. 137, 8408–8411. https://doi.org/10.1021/jacs.5b05289.

Hanstock, H.G., Edwards, J.P., Walsh, N.P., 2019. Tear lactoferrin and lysozyme as clinically relevant biomarkers of mucosal immune competence. Front. Immunol. 10, 1178 https://doi.org/10.3389/fimmu.2019.01178.

He, L., Hu, Y., Wang, M., Yin, Y., 2012. Determination of solvation layer thickness by a magnetophotonic approach. ACS Nano 6, 4196–4202. https://doi.org/10.1021/nn3007288.

Hou, Y., Lv, C.-C., Guo, Y.-L., Ma, X.-H., Liu, W., Jin, Y., Li, B.-X., Yang, M., Yao, S.-Y., 2022. Recent advances and applications in paper-based devices for point-of-care testing. J. Anal. Test. 6, 247–273. https://doi.org/10.1007/s41664-021-00204-w.

Hu, X., Li, G., Huang, J., Zhang, D., Qiu, Y., 2007. Construction of self-reporting specific chemical sensors with high sensitivity. Adv. Mater. 19, 4327–4332. https://doi.org/10.1002/adma.200701084.

Hu, Y., Yang, D., Huang, S., 2019. Amorphous photonic structures with brilliant and noniridescent colors via polymer-assisted colloidal assembly. ACS Omega 4, 18771–18779. https://doi.org/10.1021/acsomega.9b02734.

Hu, Y., Zhang, Y., Yang, D., Ma, D., Huang, S., 2021. Self-assembly of colloidal particles into amorphous photonic crystals. Mater. Adv. 2, 6499–6518. https://doi.org/10.1039/D1MA00477H.

Hyon, J., Seo, C., Nam, J., Kwon, T., Kim, J., Chung, J., Kang, Y., 2015. Enhancement of reflectance and color gamut of quasi-amorphous photonic solution by surface modification of SiO2 nanoparticles with polydopamine. Sci. Adv. Mater. 7, 881–885. https://doi.org/10.1166/sam.2015.1898.

Iguchi, M., Yamanaka, S., Watanabe, K., Nishi, Y., Uryu, M., 1991. Preparation of high-strength materials from bacterial cellulose. In: Lemstra, P.J., Kleintjens, L.A. (Eds.), Integration of Fundamental Polymer Science and Technology—5. Springer Netherlands, Dordrecht, pp. 371–379. https://doi.org/10.1007/978-94-011-3890-1_48.

Inan, H., Poyraz, M., Inci, F., Lifson, M.A., Baday, M., Cunningham, B.T., Demirci, U., 2017. Photonic crystals: emerging biosensors and their promise for point-of-care applications. Chem. Soc. Rev. 46, 366–388. https://doi.org/10.1039/C6CS00206D.

Jiang, L., Li, Y., Wang, L., Guo, J., Liu, W., Meng, G., Zhang, L., Li, M., Cong, L., Sun, M., 2021. Recent insights into the prognostic and therapeutic applications of lysozymes. Front. Pharmacol. 12, 767642. https://doi.org/10.3389/fphar.2021.767642.

Jiang, Q., Derami, H.G., Ghim, D., Cao, S., Jun, Y.-S., Singamaneni, S., 2017. Polydopamine-filled bacterial nanocellulose as a biodegradable interfacial photothermal evaporator for highly efficient solar steam generation. J. Mater. Chem. 5, 18397–18402. https://doi.org/10.1039/C7TA04834C.

Johansson, B.G., Malmquist, J., 1971. Quantitative immunochemical determination of lysoqyme (muramidase) in serum and urine. Scand. J. Clin. Lab. Invest. 27, 255–261. https://doi.org/10.3109/00365517109080216.

Jun, Y.-S., Wu, X., Ghim, D., Jiang, Q., Cao, S., Singamaneni, S., 2019. Photothermal membrane water treatment for two worlds. Acc. Chem. Res. 52, 1215–1225. https://doi.org/10.1021/acs.accounts.9b00012.

Kamel, S., Khattab, T.A., 2020. Recent advances in cellulose-based biosensors for medical diagnosis. Biosensors 10. https://doi.org/10.3390/bios10060067.

Kawamura, A., Kohri, M., Morimoto, G., Nannichi, Y., Taniguchi, T., Kishikawa, K., 2016. Full-color biomimetic photonic materials with iridescent and non-iridescent structural colors. Sci. Rep. 6, 33984 https://doi.org/10.1038/srep33984.

Lee, H., Dellatore, S.M., Miller, W.M., Messersmith, P.B., 2007. Mussel-inspired surface chemistry for multifunctional coatings. Science 318, 426–430. https://doi.org/10.1126/science.1147241.

Lee, M.-H., Chen, Y.-C., Ho, M.-H., Lin, H.-Y., 2010. Optical recognition of salivary proteins by use of molecularly imprinted poly(ethylene-co-vinyl alcohol)/quantum dot composite nanoparticles. Anal. Bioanal. Chem. 397, 1457–1466. https://doi.org/10.1007/s00216-010-3631-x.

Lee, W.-C., Ng, H.-Y., Hou, C.-Y., Lee, C.-T., Fu, L.-M., 2021. Recent advances in lab-on-paper diagnostic devices using blood samples. Lab Chip 21, 1433–1453. https://doi.org/10.1039/D0LC01304H.

Leto, G., Sepporta, M.V., 2020. The potential of cystatin C as a predictive biomarker in breast cancer. Expert Rev. Anticancer Ther. 20, 1049–1056. https://doi.org/10.1080/14737140.2020.1829481.

Li, C., Xian, J., Hong, J., Cao, X., Zhang, C., Deng, Q., Qin, Z., Chen, M., Zheng, X., Li, M., Hou, J., Zhou, Y., Yin, X., 2022. Dual photothermal nanocomposites for drug-resistant infectious wound management. Nanoscale 14, 11284–11297. https://doi.org/10.1039/D2NR01998A.

Lin, H.-Y., Ho, M.-S., Lee, M.-H., 2009. Instant formation of molecularly imprinted poly (ethylene-co-vinyl alcohol)/quantum dot composite nanoparticles and their use in one-pot urinalysis. MIP2008 Kobe, Japan, September 2008 Biosens. Bioelectron. 25, 579–586. https://doi.org/10.1016/j.bios.2009.03.039.

Liu, F., Huang, S., Xue, F., Wang, Y., Meng, Z., Xue, M., 2012. Detection of organophosphorus compounds using a molecularly imprinted photonic crystal. Biosens. Bioelectron. 32, 273–277. https://doi.org/10.1016/j.bios.2011.11.012.

Liu, P., Bai, L., Yang, J., Gu, H., Zhong, Q., Xie, Z., Gu, Z., 2019. Self-assembled colloidal arrays for structural color. Nanoscale Adv. 1, 1672–1685. https://doi.org/10.1039/C8NA00328A.

Loget, G., Yoo, J.E., Mazare, A., Wang, L., Schmuki, P., 2015. Highly controlled coating of biomimetic polydopamine in TiO2 nanotubes. Electrochem. Commun. 52, 41–44. https://doi.org/10.1016/j.elecom.2015.01.011.

Lokhande, P.E., Singh, P.P., Vo, D.-V.N., Kumar, D., Balasubramanian, K., Mubayi, A., Srivastava, A., Sharma, A., 2022. Bacterial nanocellulose: green polymer materials for high performance energy storage applications. J. Environ. Chem. Eng. 10, 108176 https://doi.org/10.1016/j.jece.2022.108176.

Luger, T., Kokoschka, E.M., Sagaster, P., Micksche, M., 1979. Serum lysozyme levels in patients with solid tumors. Oncology 36, 15–18. https://doi.org/10.1159/000225311.

Okada, Y., 2017. Chapter 8 - proteinases and matrix degradation. In: Firestein, G.S., Budd, R.C., Gabriel, S.E., McInnes, I.B., O'Dell, J.R. (Eds.), Kelley and Firestein's Textbook of Rheumatology, tenth ed. Elsevier, pp. 106–125. https://doi.org/10.1016/B978-0-323-31696-5.00008-5.

Phillips, K.R., England, G.T., Sunny, S., Shirman, E., Shirman, T., Vogel, N., Aizenberg, J., 2016. A colloidoscope of colloid-based porous materials and their uses. Chem. Soc. Rev. 45, 281–322. https://doi.org/10.1039/C5CS00533G.

Postma, A., Yan, Y., Wang, Y., Zelikin, A.N., Tjipto, E., Caruso, F., 2009. Self-polymerization of dopamine as a versatile and robust technique to prepare polymer capsules. Chem. Mater. 21, 3042–3044. https://doi.org/10.1021/cm901293e.

Rai, R., Dhar, P., 2022. Biomedical engineering aspects of nanocellulose: a review. Nanotechnology 33, 362001. https://doi.org/10.1088/1361-6528/ac6fef.

Ren, X., Yang, L., Li, Y., Cheshari, E.C., Li, X., 2020. The integration of molecular imprinting and surface-enhanced Raman scattering for highly sensitive detection of lysozyme biomarker aided by density functional theory. Spectrochim. Acta. A. Mol. Biomol. Spectrosc. 228, 117764 https://doi.org/10.1016/j.saa.2019.117764.

Resende, S., Frasco, M.F., Sales, M.G.F., 2020. A biomimetic photonic crystal sensor for label-free detection of urinary venous thromboembolism biomarker. Sensor. Actuator. B Chem. 312, 127947 https://doi.org/10.1016/j.snb.2020.127947.

Sahin, O., Ziaei, A., Karaismailoğlu, E., Taheri, N., 2016. The serum angiotensin converting enzyme and lysozyme levels in patients with ocular involvement of autoimmune and infectious diseases. BMC Ophthalmol. 16, 19. https://doi.org/10.1186/s12886-016-0194-4.

Shen, P., Shi, Y., Li, R., Han, B., Ma, H., Hou, X., Zhang, Y., Jiang, L., 2022. Multi-factors cooperatively actuated photonic hydrogel aptasensors for facile, label-free and colorimetric detection of lysozyme. Biosensors 12, 662. https://doi.org/10.3390/bios12080662.

Shi, X., He, J., Xie, X., Dou, R., Lu, X., 2019. Photonic crystals with vivid structure color and robust mechanical strength. Dyes Pigments 165, 137–143. https://doi.org/10.1016/j.dyepig.2019.02.023.

Soares da Silva, F.A.G., Matos, M., Dourado, F., A M Reis, M., C Branco, P., Poças, F., Gama, M., 2022. Development of a layered bacterial nanocellulose-PHBV composite for food packaging. J. Sci. Food Agric. 1 https://doi.org/10.1002/jsfa.11839.

Stöber, W., Fink, A., Bohn, E., 1968. Controlled growth of monodisperse silica spheres in the micron size range. J. Colloid Interface Sci. 26, 62–69. https://doi.org/10.1016/0021-9797(68)90272-5.

Vukusic, P., Sambles, J.R., 2003. Photonic structures in biology. Nature 424, 852–855. https://doi.org/10.1038/nature01941.

Wahid, F., Zhao, X.-J., Zhao, X.-Q., Ma, X.-F., Xue, N., Liu, X.-Z., Wang, F.-P., Jia, S.-R., Zhong, C., 2021. Fabrication of bacterial cellulose-based dressings for promoting infected wound healing. ACS Appl. Mater. Interfaces 13, 32716–32728. https://doi.org/10.1021/acsami.1c06986.

Wan, L., Chen, Z., Huang, C., Shen, X., 2017. Core–shell molecularly imprinted particles. TrAC, Trends Anal. Chem. 95, 110–121. https://doi.org/10.1016/j.trac.2017.08.010.

Wang, J., Pinkse, P.W.H., Segerink, L.I., Eijkel, J.C.T., 2021. Bottom-up assembled photonic crystals for structure-enabled label-free sensing. ACS Nano 15, 9299–9327. https://doi.org/10.1021/acsnano.1c02495.

Wang, L., Wang, H., Tang, X., Zhao, L., 2022. Molecularly imprinted polymers-based novel optical biosensor for the detection of cancer marker lysozyme. Sens. Actuators Phys. 334, 113324 https://doi.org/10.1016/j.sna.2021.113324.

Wang, Z., Meng, Z., Xue, M., Zhang, H., Shea, K.J., Kang, L., 2020. Detection of lysozyme in body fluid based on two-dimensional colloidal crystal sensor. Microchem. J. 157, 105073 https://doi.org/10.1016/j.microc.2020.105073.

Wei, Q., Zhang, F., Li, J., Li, B., Zhao, C., 2010. Oxidant-induced dopamine polymerization for multifunctional coatings. Polym. Chem. 1, 1430–1433. https://doi.org/10.1039/C0PY00215A.

Wu, H., Cao, D., Liu, T., Zhao, J., Hu, X., Li, N., 2015. Purification and characterization of recombinant human lysozyme from eggs of transgenic chickens. PLoS One 10, e0146032. https://doi.org/10.1371/journal.pone.0146032.

Xia, Z., Lin, Z., Xiao, Y., Wang, L., Zheng, J., Yang, H., Chen, G., 2013. Facile synthesis of polydopamine-coated molecularly imprinted silica nanoparticles for protein recognition and separation. Biosens. Bioelectron. 47, 120–126. https://doi.org/10.1016/j.bios.2013.03.024.

Xiao, M., Hu, Z., Wang, Z., Li, Y., Tormo, A.D., Le Thomas, N., Wang, B., Gianneschi, N. C., Shawkey, M.D., Dhinojwala, A., 2017. Bioinspired bright noniridescent photonic melanin supraballs. Sci. Adv. 3, e1701151 https://doi.org/10.1126/sciadv.1701151.

Yang, B., Lv, S., Chen, F., Liu, C., Cai, C., Chen, C., Chen, X., 2016. A resonance light scattering sensor based on bioinspired molecularly imprinted polymers for selective detection of papain at trace levels. Anal. Chim. Acta 912, 125–132. https://doi.org/10.1016/j.aca.2016.01.030.

Zhang, Y., Han, P., Zhou, H., Wu, N., Wei, Y., Yao, X., Zhou, J., Song, Y., 2018a. Highly brilliant noniridescent structural colors enabled by graphene nanosheets containing graphene quantum dots. Adv. Funct. Mater. 28, 1802585. https://doi.org/10.1002/adfm.201802585.

Zhang, J., Shang, M., Gao, Y., Yan, J., Song, W., 2020. High-performance VS2 QDs-based type II heterostructured photoanode for ultrasensitive aptasensing of lysozyme. Sensor. Actuator. B Chem. 304, 127411 https://doi.org/10.1016/j.snb.2019.127411.

Zhang, W., Gu, J., Liu, Q., Su, H., Fan, T., Zhang, D., 2014. Butterfly effects: novel functional materials inspired from the wings scales. Phys. Chem. Chem. Phys. 16, 19767–19780. https://doi.org/10.1039/C4CP01513D.

Zhang, X., Tang, B., Li, Y., Liu, C., Jiao, P., Wei, Y., 2021. Molecularly imprinted magnetic fluorescent nanocomposite-based sensor for selective detection of lysozyme. Nanomaterials 11, 1575. https://doi.org/10.3390/nano11061575.

Zhang, Yang, S., Jiang, R., Sun, L., Pang, S., Luo, A., 2018b. Fluorescent molecularly imprinted membranes as biosensor for the detection of target protein. Sensor. Actuator. B Chem. 254, 1078–1086. https://doi.org/10.1016/j.snb.2017.07.205.

Zhao, Y.-J., Zhao, X.-W., Hu, J., Li, J., Xu, W.-Y., Gu, Z.-Z., 2009. Multiplex label-free detection of biomolecules with an imprinted suspension array. Angew. Chem. Int. Ed. 48, 7350–7352. https://doi.org/10.1002/anie.200903472.

Zhou, C., Wang, T., Liu, J., Guo, C., Peng, Y., Bai, J., Liu, M., Dong, J., Gao, N., Ning, B., Gao, Z., 2012. Molecularly imprinted photonic polymer as an optical sensor to detect chloramphenicol. Analyst 137, 4469–4474. https://doi.org/10.1039/C2AN35617A.